

University of Nebraska - Lincoln  
**DigitalCommons@University of Nebraska - Lincoln**

---

Peter Dowben Publications

Research Papers in Physics and Astronomy

---

2011

# Schottky barrier formation at the Au to rare earth doped GaN thin film interface

S. R. McHale

*Air Force Institute of Technology*, [stephen.mchale@afit.edu](mailto:stephen.mchale@afit.edu)

J. W. McClory

*Air Force Institute of Technology*, [john.mcclory@afit.edu](mailto:john.mcclory@afit.edu)

J. C. Petrosky

*Air Force Institute of Technology*, [James.Petrosky@afit.edu](mailto:James.Petrosky@afit.edu)

J. Wu


*University of Puerto Rico*

R. Palai

*University of Puerto Rico*

*See next page for additional authors*

Follow this and additional works at: <https://digitalcommons.unl.edu/physicsdowben>

 Part of the [Atomic, Molecular and Optical Physics Commons](#), [Condensed Matter Physics Commons](#), [Engineering Physics Commons](#), and the [Other Physics Commons](#)

---

McHale, S. R.; McClory, J. W.; Petrosky, J. C.; Wu, J.; Palai, R.; Losovyj, Yaroslav B.; and Dowben, Peter A., "Schottky barrier formation at the Au to rare earth doped GaN thin film interface" (2011). *Peter Dowben Publications*. 251.

<https://digitalcommons.unl.edu/physicsdowben/251>

This Article is brought to you for free and open access by the Research Papers in Physics and Astronomy at DigitalCommons@University of Nebraska - Lincoln. It has been accepted for inclusion in Peter Dowben Publications by an authorized administrator of DigitalCommons@University of Nebraska - Lincoln.

---

**Authors**

S. R. McHale, J. W. McClory, J. C. Petrosky, J. Wu, R. Palai, Yaroslav B. Losovyj, and Peter A. Dowben

# Schottky barrier formation at the Au to rare earth doped GaN thin film interface

S.R. McHale<sup>1,a</sup>, J.W. McClory<sup>1,b</sup>, J.C. Petrosky<sup>1</sup>, J. Wu<sup>2</sup>, A. Rivera<sup>2</sup>, R. Palai<sup>2</sup>, Ya.B. Losovyj<sup>3</sup>, and P.A. Dowben<sup>4</sup>

<sup>1</sup> Air Force Institute of Technology, 2950 Hobson Way, Wright Patterson Air Force Base, OH 45433, USA

<sup>2</sup> Department of Physics and Institute for Functional Nanomaterials, University of Puerto Rico, San Juan, PR 00931-3343, USA

<sup>3</sup> The J. Bennett Johnston Sr. Center for Advanced Microstructures and Devices, Louisiana State University, 6890 Jefferson Highway, Baton Rouge, LA 70806, USA

<sup>4</sup> Department of Physics and Astronomy, Nebraska Center for Materials and Nanoscience, University of Nebraska, P.O. Box 880111, Lincoln, NE 68588-0111, USA

Received: 23 February 2010 / Accepted: 31 March 2011  
Published online: 18 August 2011 – © EDP Sciences 2011

**Abstract.** The Schottky barriers formed at the interface between gold and various rare earth doped GaN thin films (RE = Yb, Er, Gd) were investigated in situ using synchrotron photoemission spectroscopy. The resultant Schottky barrier heights were measured as  $1.68 \pm 0.1$  eV (Yb:GaN),  $1.64 \pm 0.1$  eV (Er:GaN), and  $1.33 \pm 0.1$  eV (Gd:GaN). We find compelling evidence that thin layers of gold do not wet and uniformly cover the GaN surface, even with rare earth doping of the GaN. Furthermore, the trend of the Schottky barrier heights follows the trend of the rare earth metal work function.

## 1 Introduction

During the past decade, rare earth doped semiconductors have generated considerable attention for their application in new optoelectronic devices [1–4]. The favorable thermal, chemical, and electronic properties of wide band gap, III-nitride semiconductors suggest device feasibility using lanthanide-doped AlN and GaN. Moreover, the tunable band gaps of these III-nitride alloys offer device applications across the visible spectrum through the ultraviolet range, to include optically stimulated lasing [5] and *p-n* junction light-emitting diodes in the red [6] using lanthanide-doped AlN and GaN, as well as in the blue. Lastly, the production of thin film electroluminescent phosphors with red, blue, and green emissions [7–9] offers the promise of full color (white) light capability.

The large band gap ( $\sim 3.45$  eV) of GaN minimizes the effects of thermal or visible (or longer wavelength) light charge carrier generation, while alloying with a rare earth nitride should decrease the band gap. As a general rule, the rare earth mononitrides have band gaps of 0.7–1.0 eV [10], and in many cases are suspected to be semimetals, but if alloyed with AlN or GaN are of considerable interest as semiconductors. As a device material,  $\text{RE}_x\text{Ga}_{1-x}\text{N}$  is unlikely in principle to result in significant changes to the barrier heights and the band gap of GaN, if the RE-doping level is low. Although, if metal induced gaps states

play a significant role [11, 12], even a small amount of rare earth could have a significant effect on the Schottky barrier heights. It is important to recognize that rare earth dopant induced strain, and a bulk concentration of even a dilute amount of rare earth atoms, can significantly alter the surface chemistry and the surface enthalpy leading to a means for adjusting Schottky barrier heights that can accompany an engineering of the GaN optical properties.

Although gold is generally considered unreactive [13] complications abound. Surface alloying can occur [14] and a large range of experimentally measured Schottky barrier heights has been reported (0.76–1.40 eV) at the Au to *n*-type GaN interface [13–29], using photoemission spectroscopy (PES), current-voltage (*I-V*) and capacitance voltage (*C-V*) characteristics, and internal photoemission [30]. However, the generally accepted value is about 1.08 eV [31]. Kurtin et al. [32] suggested that the Schottky barrier height on GaN should depend directly on the work function or electronegativity difference between the metal electrode and GaN. Foresi and Moustakas [33] observed this direct correlation experimentally, while Guo et al. [34] and Mori et al. [35] observed only a weak dependence of the Schottky barrier height on the metal work function for *n*-type GaN and *p*-type GaN, respectively. The 1998 review of metal-GaN contact technology by Liu and Lau [19] reported that, for a variety of contact metals with both low and high work functions, Schottky barrier heights at the metal-GaN interface varied with metal work function, within the experimental scatter. Subsequent work

<sup>a</sup> e-mail: stephen.mchale@afit.edu

<sup>b</sup> e-mail: john.mcclory@afit.edu

by Rickert et al. [23] supported a modified Schottky-Mott model at the metal-GaN interface for Ni, Pd, and Al, yet more ‘complex’ behavior when Au, Ti, and Pt were used as the contact metals. Additional experiments by Barinov et al. [21,22] reported Schottky barrier heights at the Au-GaN interface that exceeded both work function difference (Schottky-Mott) and electronegativity difference (metal induced gap states) models. Thus, a point worth re-emphasizing is that regardless of the particular metal-GaN interface studied, experimentally measured barrier heights vary considerably.

Using photoemission to measure the surface barrier height is advantageous because the technique is both extremely surface sensitive, and one can avoid some of the complications associated with other experimental techniques. For example when using traditional  $I$ - $V$  and  $C$ - $V$  measurements, defects at the metal-semiconductor interface can often lead to overestimates of the surface barrier height [23,36].

Although likely to locally strain the lattice, the 4f rare earths will tend to adopt substitutional sites for Ga [1,2,37] in GaN while significantly altering magnetic and optical properties [10], and it is of considerable interest to know whether even low concentrations of a rare earth in the GaN host will routinely lead to high or low barrier height values at the Au-RE:GaN interface. With this in mind, we have engaged in investigations of the interface properties of  $\text{RE}_x\text{Ga}_{1-x}\text{N}$  (RE = Yb, Er, Gd) semiconductors with Au metal overlayer deposition under UHV conditions. Our studies of the Au to  $\text{RE}_x\text{Ga}_{1-x}\text{N}$  semiconductor interface properties were performed much in the manner of other studies of the Au to GaN interface [18,20–23].

## 2 Experimental

The  $\text{RE}_x\text{Ga}_{1-x}\text{N}$  thin films (50–300 nm) were fabricated on Si(1 1 1) (RE = Yb, Gd) and  $\text{Al}_2\text{O}_3$  (RE = Er) substrates by RF plasma (EPI 620) assisted molecular beam epitaxy (MBE). The growth parameters for the deposition of RE-doped (in situ) GaN thin films were base pressure of  $\sim 10^{-11}$  Torr, nitrogen flux of 0.75–1.0 SCCM (Yb, Gd) and 2.0 SCCM (Er), RF power of 500 W, substrate temperature of 850–900 °C, Ga cell temperature of 850 °C, and RE cell temperatures of 500–850 °C (Yb), 1000–1100 °C (Er), and 1050–1100 °C (Gd). The thickness of the films was measured with a surface profilometer.

The orientation, crystal structure, and phase purity of the films were established by Cu  $K_\alpha$  ( $\lambda = 1.5406$  Å) radiation X-ray diffraction using a Siemens D5000 X-ray diffractometer. The X-ray diffraction (XRD) pattern of Yb, Er and Gd-doped GaN films shows  $c$ -axis orientation and a high degree of crystallinity. The presence of any secondary phases or spurious peaks has not been observed. Slight shifts in diffraction peaks positions toward lower Bragg angles have been observed with Yb-doped GaN grown on  $\text{Al}_2\text{O}_3(0\ 0\ 0\ 1)$  substrates and  $\text{RE}_x\text{Ga}_{1-x}\text{N}$  thin films (50–300 nm) fabricated on Si(1 1 1) (RE = Yb, Gd) indicative of some lattice expansion. The  $c$ -axis length of

Yb:GaN was found to be 5.172 Å [37], which is very close to the widely reported and accepted  $c$ -axis length (5.166 Å) of undoped GaN.

The elemental compositions of the rare earth doped GaN thin films grown under different conditions were characterized by energy dispersive spectroscopy (EDS) and a VG Microtech XPS attached to the MBE growth system (VG Microtech). The measured concentrations were found to be at 1–2%, as confirmed from the Ga  $2p_{3/2}$ , Er  $4d$ , Gd  $4d$ , Yb  $4d$ , and N  $1s$  core-level XPS intensities using an Al  $K_\alpha$  (1486.8 eV) X-ray source. The typical values for Er concentrations were found to be  $\sim 5\%$ , higher than the EDS- and XPS-derived Gd and Yb concentrations. In the rare earth doped GaN samples, surface segregation cannot be excluded and may well be likely, at least in the selvedge region of the surface.

The photoemission experiments were conducted on the 3m TGM beamline [38] at the Center for Advanced Microstructures and Devices at Louisiana State University [39]. The beamline is equipped with a photoemission endstation with a 50-mm hemispherical electron energy analyzer, with a resolution of about 70 meV, as described elsewhere [38,40]. Photoemission spectra were taken with a 45° incidence angle and the photoelectrons collected along the sample normal. The position of the Fermi level  $E_F$  with respect to the valence band maximum was established using a clean Ta foil as reference. All binding energies reported here are with respect to this common Fermi level.

Atomically clean RE:GaN surfaces were obtained by several preparatory cycles of  $\text{Ar}^+$  ion sputtering and annealing. This will create a number of point defects, but photoemission is generally insensitive to such defects. The photoemission spectra from the clean sample surface indicated that the surfaces were free of contaminants. The Au deposition was made by thermal evaporation on the clean RE:GaN surface at room temperature. To prevent contamination, the background vacuum pressure was generally kept at  $<10^{-9}$  Torr. The evaporation rate and average coverage, reported here in Å, were monitored by means of a quartz crystal thickness monitor located in the evaporation chamber. A low deposition rate of  $\sim 0.2$  Å/min was used in a best effort to enhance uniform film growth and ensure accurate determinations of the average Au film thickness.

## 3 Results and discussion

### 3.1 The rare earth doped GaN surfaces

The relative position of the valence band, and changes due to the band bending, were determined by monitoring the Ga  $3d$  core-level shift as a function of Au coverage. The measured Ga  $3d$  peaks in Figures 1a, 2a, and 2b are very similar to the photoemission spectra reported previously [20–22,41,42]. The Ga  $3d$  shallow core-level peaks are broad, with maxima at 17.7 eV (Yb:GaN), 17.1 eV (Er:GaN), and 17.4 eV (Gd:GaN) below the valence band

maximum (VBM), in acceptable agreement with the expected value of 17.7 eV [21, 22, 41] for wurtzite GaN. The energy difference between the valence band maximum and a core level,  $E_{\text{VBM-C}}$ , is considered a bulk property of the material and is, therefore, independent of metal coverage [21–23]. The valence band maximum, determined by extrapolation of the high kinetic energy edge of the clean spectrum, as is the common practice [20–23, 42, 43], is at 2.7 eV below  $E_{\text{F}}$  for the Yb:GaN surface. Assuming that the low RE-doping levels (1–2%) of our samples leave the 3.45 eV band gap for GaN relatively unchanged, and given that  $E_{\text{F}}$  is approximately 50 meV below the conduction band minimum in the bulk of  $n$ -type GaN [20], determines the upward band bending at the clean Yb:GaN surface (bare surface barrier height) as 0.70 eV. A consequence of the high photon flux environment ( $\geq 10^{11}$  photons  $\mu\text{m}^{-2}$   $\text{s}^{-1}$ ) required by photoelectron spectroscopy are surface photovoltage effects, which have been known to cause band flattening [21]. By varying the sample temperature in a separate experiment, we demonstrated that surface photovoltage was negligible for our samples. Thus, we consider our measured bare surface barrier height to be in good agreement with values reported previously for UHV prepared  $n$ -type wurtzite GaN surfaces (0.50–1.40 eV) [20, 21, 42–44].

The ionization energy

$$\text{IE} = E_{\text{VAC}} - E_{\text{VBM}} = (E_{\text{F}} - E_{\text{VBM}}) + \phi_{\text{A}} \quad (1)$$

given the analyzer work function  $\phi_{\text{A}}$  of 4.4 eV, is  $7.1 \pm 0.1$  eV for Yb:GaN, which is in reasonable agreement with prior values (6.7–6.9 eV) [20, 44] for GaN. The electron affinity

$$\chi = \phi_{\text{A}} - [E_{\text{G}} - (E_{\text{F}} - E_{\text{VBM}})] \quad (2)$$

is thus  $3.7 \pm 0.1$  eV for Yb:GaN, which is in reasonable agreement (2.2–4.1 eV) [20, 42, 44, 45] with previously reported results for GaN. Table 1 summarizes the experimentally measured surface electronic properties of each RE:GaN sample and indicates reasonable agreement, given the low RE-doping levels, between our samples and previously published GaN values.

### 3.2 The growth of gold overlayers on RE:GaN surfaces

Figure 1 shows the evolution of the valence band and Ga 3d spectra for a Yb:GaN sample with increasing Au coverage. The progressively metallic nature of the overlayer film is reflected in the valence band features by a density of states above the valence band maximum at a Au overlayer film thickness of about 6 Å, leading to emission at or near the Fermi level ( $E_{\text{F}}$ ) at about 12 Å of Au. The valence band of the gold overlayer, as seen in the photoemission data, is dominated by the Au 5d weighted bands [46], as is expected, with the Au 5d levels at binding energies of 3.5 and 6.1 eV, in reasonable agreement with published values for bulk Au [47] and gold deposited on III-V semiconductors [48].

We also measured the Au 4 $f_{7/2}$  and Au 4 $f_{5/2}$  levels as a function of Au coverage, as shown in Figure 1b. The Au 4f

features appear, at a coverage of 4 Å, at binding energies that are approximately 0.3 eV greater than the Au 4 $f_{7/2}$  and Au 4 $f_{5/2}$  levels of 84.0 eV and 87.7 eV in metallic Au [49]. With increasing Au coverage up to 16 Å, these peaks sharpen, increase in intensity, and shift toward the lower binding energies of bulk Au. This decrease in the Au 4 $f_{7/2}$  and Au 4 $f_{5/2}$  levels, with increasing gold coverage, is one of many indicators that initial gold adsorption is not uniformly wetting the surface and that island growth is likely.

From photoemission work with Au alloys, it is known that Au surface distribution may be probed by following the details of the 5d bands [50]. When Au atoms are well dispersed, as in a dilute Au alloy, 5d bands are shifted toward higher binding energies, as compared to the bulk values. The splitting of the 5d valence band features should increase from the value for atomic Au (1.5 eV) to the bulk value (2.5 eV) with increased deposition. In our studies, we find the Au 5d band splitting is about 2.6 eV for Yb:GaN (Fig. 1b) and Gd:GaN (Fig. 2b), almost independent of Au overlayer coverage, indicative of rapid metallic Au island formation.

Attenuation of the Ga 3d core level in Figures 1a, 2a, and 2b (RE = Yb, Er, Gd) also indicates that the growth mode of the Au on the respective RE:GaN surfaces is not uniform (Frank-van der Merwe or layer-by-layer growth) but rather the Au overlayer growth follows Volmer-Weber (island growth) or Stranski-Krastanov growth. While the growth mode strongly depends on the particular metal-semiconductor pair and also on the experimental conditions such as substrate temperature and evaporation rate [51], the evidence for Volmer-Weber (island growth) or Stranski-Krastanov growth in describing Au on the respective RE:GaN surfaces is robust. If the gold were of uniform thickness, the Ga 3d core-level photoemission signal would be absent at thicker Au overlayer coverages due to the limited mean free path of approximately 5 Å in Au [52, 53], estimated from the kinetic energy of a Ga 3d photoelectron using a photon energy of 90 eV.

Since the Ga 3d core levels are visible in the spectra up to 16 Å Au coverage, thin spots must exist in the Au overlayer film. The intensity of the Ga 3d core level before  $I_0$  and after  $I_s$  deposition leads to a change in photoemission intensity, described by Volmer-Weber growth [23, 51, 54, 55], as

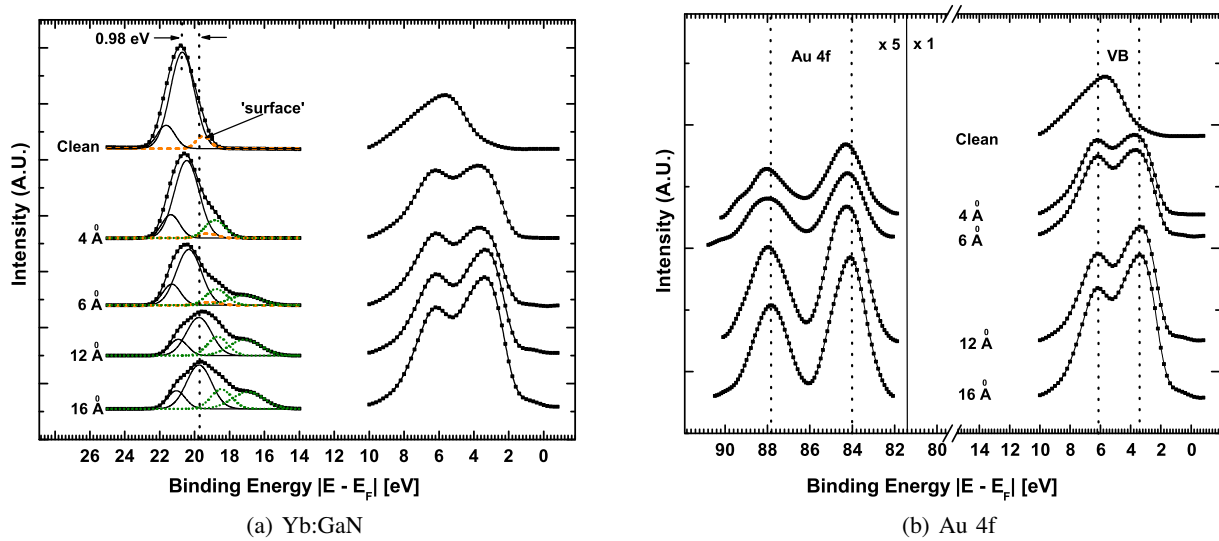
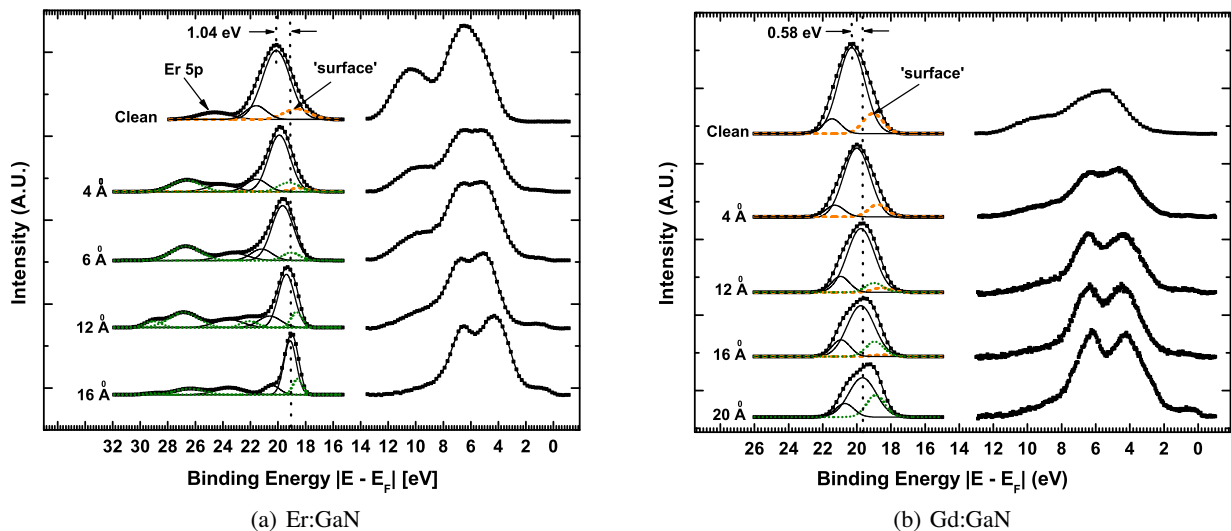
$$\frac{I_s}{I_0} = (1 - \theta) + \theta e^{-t/\lambda}, \quad (3)$$

where  $t$  is the film thickness,  $\lambda$  is the mean free path of the electrons, and  $\theta$  represents the fractional surface coverage reached prior to island growth in three dimensions. Figure 3 shows the photoemission intensity ratios of the Ga 3d core level for each of the RE:GaN thin films studied. As expected, the fit parameter differs for each Au to RE:GaN interface studied, which reflects the strong growth mode dependence upon the particular metal-semiconductor pair.

The data indicate that Au is not growing in a layer-by-layer manner but rather by Volmer-Weber (island growth)

**Table 1.** Measured properties of clean RE:GaN surfaces. Experimental uncertainties are listed only when explicitly stated within the indicated references.

Material	$E_F - E_{VBM}$	BSBH	IE	$\chi$
Yb:GaN	$2.70 \pm 0.1$	$0.70 \pm 0.1$	$7.10 \pm 0.1$	$3.70 \pm 0.1$
Er:GaN	$2.80 \pm 0.1$	$0.60 \pm 0.1$	$7.20 \pm 0.1$	$3.80 \pm 0.1$
Gd:GaN	$2.65 \pm 0.1$	$0.75 \pm 0.1$	$7.05 \pm 0.1$	$3.65 \pm 0.1$
GaN	2.60 [20]	$0.75 \pm 0.1$ [20]	$6.90 \pm 0.1$ [20]	$3.50 \pm 0.1$ [20]
GaN	$2.80 \pm 0.1$ [21]	$0.50 \pm 0.1$ [21]		
GaN	$1.90 \pm 0.2$ [42]	$1.40 \pm 0.2$ [42]		$2.70 \pm 0.2$ [42]
GaN	2.70 [43]	0.70 [43]		2.20–4.10 [45]
GaN	2.50 [44]	0.90 [44]	6.70 [44]	3.30 [44]


**Fig. 1.** (Color online) (a) Deconvolution of Ga  $3d$  core-level spectra and (b) evolution of valence band and Au  $4f$  bands with increasing Au coverage on Yb:GaN thin film. The components attributed to bulk GaN features are shown with solid lines. The lower binding energy ‘surface’ component (dashed line) is removed with increasing Au coverage and is replaced with Au-GaN and Au-RE alloy features (dotted lines).

**Fig. 2.** (Color online) Deconvolution of Ga  $3d$  core-level spectra and valence band evolution with increasing Au coverage on (a) Er:GaN and (b) Gd:GaN thin films. The components attributed to bulk GaN features are shown with solid lines. The lower binding energy ‘surface’ component (dashed line) is removed with increasing Au coverage and is replaced with Au-GaN and Au-RE alloy features (dotted lines).

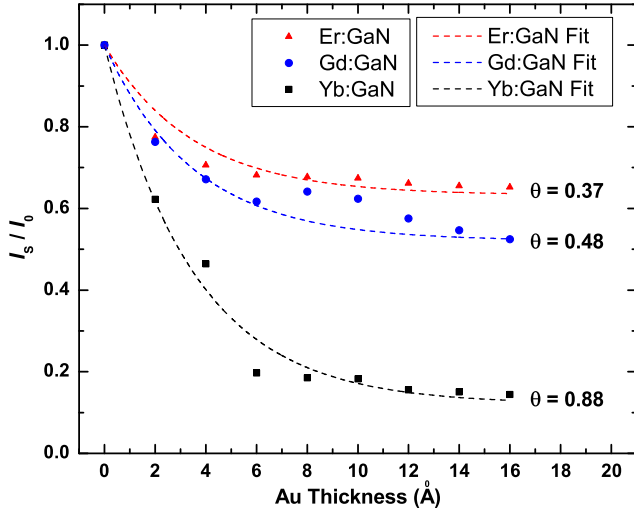




**Fig. 3.** (Color online) The intensity ratio of the Ga 3d core level before  $I_0$  and after  $I_s$  Au deposition as a function of film thickness for the deposition of Au on RE:GaN, as indicated. The expected ratio as a function of thickness (dashed lines) is plotted using the Volmer-Weber growth mode.

or Stranski-Krastanov growth. Although layer-by-layer growth for Au on GaN has been reported [18], there has also been evidence of island formation [18, 23, 56]. Here, we find compelling evidence that thin layers of gold do not wet and cover the GaN surface, even with rare earth doping of the GaN. We would expect that a dilute surface coverage of rare earth atoms would nucleate more uniform Au overlayer films, but this does not appear to be the case.

### 3.3 Schottky barrier formation at RE:GaN surfaces

When metal is evaporated on the sample surface, the edge of the semiconductor valence band maximum is obscured by the signal originating from the metal overlayer. However, owing to the fact that  $E_{\text{VBM-C}}$  is constant, the Ga 3d core shift results in an equivalent valence band shift at the semiconductor surface, from which the Schottky barrier height  $\Phi_{\text{B,n}}$  is calculated as

$$\Phi_{\text{B,n}} = E_{\text{G}} - (E_{\text{F}} - E_{\text{VBM}}). \quad (4)$$

To describe the surface Fermi level movement and Schottky barrier formation during Au deposition, Ga 3d core levels were deconvoluted into surface and bulk components with Gaussian form. There exists some variation concerning the number of fitting components for the Ga 3d lineshape. Some authors choose a single, dominant bulk subpeak and one surface subpeak [41, 57] to represent the surface to bulk core-level shift that affects the Ga 3d lineshape, whereas other researchers deconvolute the lineshape using two bulk subpeaks and one surface subpeak [21, 22, 58]. We calculated Schottky barrier heights using both methods, and their differences proved negligible ( $<0.05$  eV)

for all Au to RE:GaN interfaces. However, we present only our results using the latter method to deconvolute the Ga 3d peak, as this is deemed more reliable. We selected this method owing to the compelling arguments of Barinov et al. [21, 22] and Lambrecht et al. [58] who demonstrated that the dominant and high binding energy components of the peak are intrinsic features of the Ga 3d semi-core levels of GaN and are related to hybridization effects [19], while the lower binding energy component behaves as a ‘surface’ component. In Figures 1, 2a, and 2b, solid subpeaks represent bulk components and dashed subpeaks represent the surface components. As Au coverage increases, Au forms a surface alloy with GaN and RE metals on the sample surface, and their features are represented as dotted subpeaks. These features supplant the surface component of the Ga 3d core levels.

The effect of Au deposition on the various RE-doped GaN surfaces is not identical, as inferred from the Ga 3d shallow-core spectra. The clean Yb:GaN Ga 3d shallow-core spectra in Figure 1a and the clean Gd:GaN Ga 3d shallow-core spectra in Figure 2b required three fitting components to represent the Ga 3d lineshape. During Au deposition on Yb:GaN, the single surface component was replaced with two alloy/Au interface components that were separated, at lower binding energies, from the dominant bulk peak by 1.3 eV and 2.9 eV. During Au deposition on Gd:GaN, the single surface component was replaced with a single alloy/Au interface component that was separated, at a lower binding energy, from the dominant bulk peak by 0.7 eV.

The clean Er:GaN spectrum in Figure 2a required four subpeaks to deconvolute the Ga 3d lineshape. We associate the fourth subpeak, at binding energy 24.8 eV, with the Er 5p core level, which has a binding energy of 28.0 eV in bulk Er. During Au deposition, the single surface component was replaced with one alloy component that was separated, at a lower binding energy, from the dominant Ga 3d bulk peak by 0.6 eV. Additional fitting components were needed to deconvolute the spectral features that evolved around the Er 5p subpeak. One alloy component located, at a higher binding energy, from the Er 5p subpeak by 3.0 eV is present in all spectra from 4 Å to 16 Å Au coverage. The intensity of this Ga 3d shallow-core spectra component increases from 4 Å to 12 Å Au coverage, but is attenuated at 16 Å Au coverage, possibly the result of surface alloy formation. When this Ga 3d shallow-core spectra component is at maximum intensity at 12 Å Au coverage, precise spectral deconvolution requires two additional alloy components. These two additional alloy/Au interface components are separated from the Er 5p subpeak by lower and higher binding energies of 1.7 eV and 5.3 eV, respectively.

Fermi level movement, surface valence band bending, and Schottky barrier formation were determined by monitoring the binding energy shift of the dominant, bulk Ga 3d component during Au deposition. Figures 1a, 2a, and 2b show these measured shifts to be 0.98 eV (Yb:GaN), 1.04 eV (Er:GaN), and 0.58 eV (Gd:GaN). Figure 4 shows the surface Fermi level movement 4a and resultant Schottky barrier formation 4b for Gd:GaN, which was

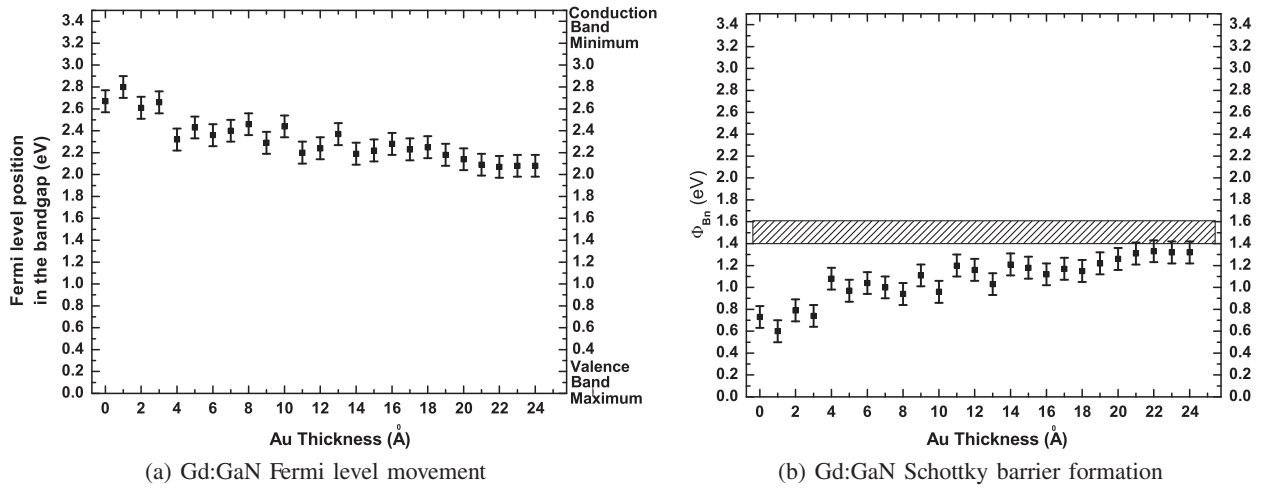


**Fig. 4.** (a) Fermi level movement and (b) Schottky Barrier formation at the surface of Gd:GaN based upon the binding energy of the bulk component of a Ga  $3d$  core level taken at a photon energy of 90 eV. The filled region in (b) indicates the range of ideal barrier height values, as predicted by the Schottky-Mott model using our measured  $\chi$  values from Table 1.

**Table 2.** Comparison between experimentally measured and theoretically predicted (Schottky-Mott) barrier heights. Experimental uncertainties are listed only when explicitly stated within the indicated references.

Material	$\chi_s$ [eV] via Table 1	$\Phi_{B,n}$ [eV] (theory)	$\Phi_{B,n}$ [eV] (measured)	Measurement technique
Yb:GaN	$3.70 \pm 0.1$	$1.45 \pm 0.1$	$1.68 \pm 0.1$	PES
Er:GaN	$3.80 \pm 0.1$	$1.35 \pm 0.1$	$1.64 \pm 0.1$	PES
Gd:GaN	$3.65 \pm 0.1$	$1.50 \pm 0.1$	$1.33 \pm 0.1$	PES
GaN	4.10 [45]	1.05	1.15 [18]	PES
GaN			$1.20 \pm 0.1$ [20]	PES
GaN			$1.40 \pm 0.1$ [21,22]	PES
GaN			$0.90 \pm 0.1$ [23]	PES
GaN			$1.18 \pm 0.07$ [25]	$I-V$
GaN			0.94 [15]	$I-V$
GaN			1.19 [16]	$I-V$
GaN			1.15 [16]	$C-V$
GaN			0.87 [17]	$I-V$
GaN			0.98 [17]	$C-V$
GaN			1.10 [13]	$I-V$
GaN			1.22 [14]	$I-V$
GaN			0.81 [28]	$I-V$
GaN			0.76 [28]	IPE
GaN			1.0 [29]	IPE
GaN			1.11 [24]	IPE
GaN			$0.95 \pm 0.04$ [26]	IPE
GaN			$0.97 \pm 0.05$ [27]	IPE

calculated as  $1.33 \pm 0.1$  eV via (4). The same methods and calculations described above yielded Schottky barrier heights of  $1.64 \pm 0.1$  eV and  $1.68 \pm 0.1$  eV for Er:GaN and Yb:GaN, respectively. These are generally far larger than the values found for undoped GaN, as measured via PES,  $I-V$ ,  $C-V$ , and internal photoemission (IPE), and summarized in Table 2.

In a separate experiment at the same facility, we measured changes in the band bending at the valence band maximum with gold evaporation on AlGaIn/GaN multilayers. The measured Schottky barrier height ( $0.86 \pm 0.1$  eV) was indeed consistent with reported values for Schottky barrier heights at Au-GaN and

Au-AlGaIn/GaN interfaces (0.9–1.1 eV). Thus, we do not attribute the larger Schottky barrier heights at the Au-RE:GaIn interfaces with the experimental arrangement.

Because of the possible interfacial reactions between the Au and RE:GaIn surfaces, the magnitude of the shift in the Ga  $3d$  shallow-core spectra due to Au charge donation cannot be determined quantitatively. While we associate the Ga  $3d$  core shift with band bending, we must be careful to state that other causes cannot be completely excluded by the data presented here.

The Schottky-Mott relationship characterizes contacts for  $n$ -type semiconductors such that when the work



function of the metal contact is greater than the work function of the semiconductor, i.e.,  $\phi_m > \phi_s$ , the contact is rectifying. The work function  $\phi_s$  for GaN has been calculated from photoemission experiments as  $4.2 \pm 0.2$  eV [43], whereas the work function  $\phi_m$  of Au is 5.15 eV [59]. The Schottky-Mott theory also predicts that for  $n$ -type semiconductors, with  $\phi_m > \phi_s$ , the surface barrier height is calculated as the difference between the contact metal work function and the electron affinity of the semiconductor sample  $\chi_s$  as

$$\Phi_{B,n} = \phi_m - \chi_s. \quad (5)$$

The most commonly used [17,33,41] electron affinity for undoped GaN was reported as 4.1 eV [45], which yields a theoretical barrier height of 1.05 eV between Au and GaN. Our measured values for  $\chi_s$ , determined from the clean RE:GaN bare surface barrier heights (Tab. 1), suggest higher theoretical Schottky barrier heights ( $1.45 \pm 0.1$  eV (Yb:GaN),  $1.35 \pm 0.1$  eV (Er:GaN),  $1.50 \pm 0.1$  eV (Gd:GaN)) than for undoped GaN (Tab. 2). Thus, both measured and theoretically predicted Au-RE:GaN Schottky barrier heights are larger than those for the Au-GaN interface. Given a constant electrode metal work function, either a decreased semiconductor electron affinity (5) or decreased semiconductor work function (increased contact potential) due to rare earth doping of GaN would produce higher barrier heights than for undoped GaN, but more likely, both occur.

We note that, in general, the trend of the Schottky barrier heights follows the trend of the rare earth metal work function, so that although the RE ion occupies a Ga site in the GaN [1,2,37], perturbation of the rare earth on the surface electronic structure of GaN is possible. The work function of Yb is 2.60 eV [60], that of Er is 2.97 eV [61], while Gd is 3.10 eV [59], all of which are lower than that of GaN (4.2 eV).

Regardless of the interplay between electron affinity and GaN surface work function, the resultant Au-RE:GaN Schottky barrier heights, as measured and noted above, are  $1.68 \pm 0.1$  eV (Yb:GaN),  $1.64 \pm 0.1$  eV (Er:GaN), and  $1.33 \pm 0.1$  eV (Gd:GaN), and are significantly higher than those observed for undoped GaN. Thus, band bending at the Au-RE:GaN (RE = Yb, Er, Gd) interface is larger than the normal (Au-GaN). This implies that barrier heights might be engineered to optimize depletion widths and charge collection volumes for sensor device applications.

## 4 Summary

Photoemission studies using synchrotron radiation showed that the Schottky barrier heights between Au and RE:GaN thin film samples were measured to be  $1.68 \pm 0.1$  eV (Yb:GaN),  $1.64 \pm 0.1$  eV (Er:GaN), and  $1.33 \pm 0.1$  eV (Gd:GaN). This trend of the Schottky barrier heights follows the trend of the rare earth metal work function. The Au overlayer does not wet and cover the GaN surface, even with rare earth doping of the GaN. But in spite

of the imperfections of the Au-RE:GaN interface, the resulting Schottky barrier interfaces might lead to significant improvement in device performance in sensor applications.

This work was supported by the Defense Threat Reduction Agency (DTRA) through Grant Nos. HDTRA1-07-1-0008 and BRBAA08-I-2-0128, the Nebraska Materials Science and Engineering Center (DMR-0820521), the Institute for Functional Nanomaterials, and NASA-IDEA-PR. Additional support for undergraduates, at UNL, was provided by DMR-0851703. The J. Bennett Johnston Sr. Center for Advanced Microstructures and Devices (CAMD) is supported by the Louisiana Board of Regents.

The views expressed in this article are those of the authors and do not reflect the official policy or position of the Air Force, Department of Defense, or the U.S. Government.

## References

1. T. Koubaa, M. Dammak, M. Kammoun, W.M. Jadwisieniczak, H.J. Lozykowski, *J. Alloys Compd.* **496**, 56 (2010)
2. T. Koubaa, M. Dammak, M. Kammoun, W.M. Jadwisieniczak, H.J. Lozykowski, A. Anders, *J. Appl. Phys.* **106**, 013106 (2009)
3. W.M. Jadwisieniczak, H.J. Lozykowski, *Opt. Mater.* **23**, 175 (2003)
4. A.J. Kenyon, *Prog. Quant. Electr.* **26**, 225 (2002)
5. J.H. Park, A.J. Steckl, *Phys. Stat. Sol. (a)* **205**, 26 (2008)
6. A. Nishikawa, T. Kawasaki, N. Furukawa, Y. Terai, Y. Fujiwara, *Appl. Phys. Express* **2**, 1004 (2009)
7. A.J. Steckl, J. Heikenfeld, D.S. Lee, M. Garter, *Mater. Sci. Eng. B* **81**, 97 (2001)
8. J.H. Tao, N. Perea-Lopez, J. McKittrick, J.B. Talbot, K. Klinedinst, M. Raukas, J. Laski, K.C. Mishra, G. Hirata, *Phys. Stat. Sol. C* **5**, 1889 (2008)
9. J. Shi, M.V.S. Chandrashekar, J. Reiherzer, W. Schaff, J. Lu, F. Disalvo, M. Spencer, *Phys. Stat. Sol. (c)* **5**, 1495 (2008)
10. C.G. Duan, R.F. Sabirianov, W.N. Mei, P.A. Dowben, S.S. Jaswal, E.Y. Tsymbal, *J. Phys.: Condens. Matter* **19**, 315220 (2007)
11. V. Heine, *Phys. Rev.* **138**, 1689 (1965)
12. T.U. Kampen, W. Mönch, *Appl. Surf. Sci.* **117**, 388 (1997)
13. Y. Kribes, I. Harrison, B. Tuck, T.S. Cheng, C.T. Foxon, *Semicond. Sci. Technol.* **12**, 913 (1997)
14. L. He, X.J. Wang, R. Zhang, *J. Vac. Sci. Technol. A: Vac. Surf. Films* **17**, 1217 (1999)
15. P. Hacke, T. Detchprohm, K. Hiramatsu, N. Sawaki, *Appl. Phys. Lett.* **63**, 2676 (1993)
16. S.C. Binari, H.B. Dietrich, G. Kelner, L.B. Rowland, K. Doverspike, D.K. Gaskill, *Electron. Lett.* **30**, 909 (1994)
17. A.C. Schmitz, A.T. Ping, M.A. Khan, Q. Chen, J.W. Yang, I. Adesida, *Semicond. Sci. Technol.* **11**, 1464 (1996)
18. R. Sporcken, C. Silien, F. Malengreau, K. Grigorov, R. Caudano, F.J. Sanchez, E. Calleja, E. Munoz, B. Beaumont, P. Gibart, *MRS Int. J. Nitride Semicond. Res.* **1** (1996)
19. Q.Z. Liu, S.S. Lau, *Solid-State Electron.* **42**, 677 (1998)

20. C.I. Wu, A. Kahn, J. Vac. Sci. Technol. B: Microelectron. Nanometer Struct. **16**, 2218 (1998)
21. A. Barinov, L. Casalis, L. Gregoratti, M. Kiskinova, Phys. Rev. B **63**, 85308 (2001)
22. A. Barinov, L. Casalis, L. Gregoratti, M. Kiskinova, J. Phys. D: Appl. Phys. **34**, 279 (2001)
23. K.A. Rickert, A.B. Ellis, J.K. Kim, J.L. Lee, F.J. Himpsel, F. Dwikusuma, T.F. Kuech, J. Appl. Phys. **92**, 6671 (2002)
24. A.R. Arehart, B. Moran, J.S. Speck, U.K. Mishra, S.P. DenBaars, S.A. Ringel, J. Appl. Phys. **100**, 023709 (2006)
25. E. Monroy, F. Calle, T. Palacios, J. Sánchez-Osorio, M. Verdú, F.J. Sánchez, M.T. Montojo, F. Omnès, Z. Bougrioua, I. Moerman, Phys. Stat. Sol. (a) **188**, 367 (2001)
26. W. Götz, N.M. Johnson, R.A. Street, H. Amano, I. Akasaki, Appl. Phys. Lett. **66**, 1340 (1995)
27. D. Qiao, L.S. Yu, S.S. Lau, J.M. Redwing, J.Y. Lin, H.X. Jiang, J. Appl. Phys. **87**, 801 (2000)
28. F. Binet, J.Y. Duboz, N. Laurent, E. Rosencher, O. Briot, R.L. Aulombard, J. Appl. Phys. **81**, 6449 (1997)
29. I. Shalish, L. Kronik, G. Segal, Y. Shapira, M. Eizenberg, J. Salzman, Appl. Phys. Lett. **77**, 987 (2000)
30. R.H. Fowler, Phys. Rev. **38**, 45 (1931)
31. S. Picozzi, A. Continenza, G. Satta, S. Massidda, A.J. Freeman, Phys. Rev. B **61**, 16736 (2000)
32. S. Kurtin, T.C. McGill, C.A. Mead, Phys. Rev. Lett. **22**, 1433 (1969)
33. J.S. Foresi, T.D. Moustakas, Appl. Phys. Lett. **62**, 2859 (1993)
34. J.D. Guo, M.S. Feng, R.J. Guo, F.M. Pan, C.Y. Chang, Appl. Phys. Lett. **67**, 2657 (1995)
35. T. Mori, T. Kozawa, T. Ohwaki, Y. Taga, S. Nagai, S. Yamasaki, S. Asami, N. Shibata, M. Koike, Appl. Phys. Lett. **69**, 3537 (1996)
36. D.K. Schroder, *Semiconductor Material and Device Characterization* (John Wiley & Sons, 1990)
37. S.R. McHale, J.W. McClory, J.C. Petrosky, J. Wu, R. Palai, P.A. Dowben, I. Ketsman, Mater. Lett. **65**, 1476 (2011)
38. Y. Losovyj, I. Ketsman, E. Morikawa, Z. Wang, J. Tang, P. Dowben, Nucl. Instr. Methods A **582**, 264 (2007)
39. J. Hormes, J.D. Scott, V.P. Suller, Synchrotron Radiat. News **19**, 27 (2006)
40. P.A. Dowben, D. LaGraffe, M. Onellion, J. Phys.: Condens. Matter **1**, 6571 (1989)
41. M.H. Kim, S.N. Lee, C. Huh, S.Y. Park, J.Y. Han, J.M. Seo, S.J. Park, Phys. Rev. B **61**, 10966 (2000)
42. V.M. Bermudez, T.M. Jung, K. Doverspike, A.E. Wickenden, J. Appl. Phys. **79**, 110 (1996)
43. V.M. Bermudez, D.D. Koleske, A.E. Wickenden, Appl. Surf. Sci. **126**, 69 (1998)
44. W. Xiao, Q. Guo, Q. Xue, E.G. Wang, J. Appl. Phys. **94**, 4847 (2003)
45. J.I. Pankove, H. Schade, Appl. Phys. Lett. **25**, 53 (1974)
46. M.G. Ramchandani, J. Phys. C: Solid State Phys. **3**, S1 (1970)
47. H. Ebel, N. Gurker, Phys. Lett. A **50**, 449 (1975)
48. L. Ley, R.A. Pollak, F.R. McFeely, S.P. Kowalczyk, D.A. Shirley, Phys. Rev. B **9**, 600 (1974)
49. S. Hüfner, *Photoelectron Spectroscopy: Principles and Applications* (Springer Verlag, Germany, 2003)
50. P.W. Chye, I. Lindau, P. Pianetta, C.M. Garner, C.Y. Su, W.E. Spicer, Phys. Rev. B **18**, 5545 (1978)
51. W. Mönch, *Semiconductor Surfaces and Interfaces* (Springer Verlag, Berlin, 2001)
52. D.R. Penn, Phys. Rev. B **35**, 482 (1987)
53. M.P. Seah, W.A. Dench, Surf. Interface Anal. **1**, 2 (1979)
54. J. Venable, *Introduction to Surface and Thin Film Processes* (Cambridge University Press, 2000)
55. J.A. Venables, Surf. Sci. **299**, 798 (1994)
56. Q.Z. Liu, K.V. Smith, E.T. Yu, S.S. Lau, N.R. Perkins, T.F. Keuch, Mater. Res. Soc. Symp. Proc. **449**, 1079 (1997)
57. G.L. Lay, D. Mao, A. Kahn, Y. Hwu, G. Margaritondo, Phys. Rev. B **43**, 14301 (1991)
58. W.R.L. Lambrecht, B. Segall, S. Strite, G. Martin, A. Agarwal, H. Morkoc, A. Rockett, Phys. Rev. B **50**, 14155 (1994)
59. D.E. Eastman, Phys. Rev. B **2**, 1 (1970)
60. M.V. Nikolic, S.M. Radi, V. Mini, M.M. Risti, Microelectron. J. **27**, 93 (1996)
61. E.M. Savitskiy, V.F. Terekhova, E.V. Maslova, Radio Eng. Electron. Phys. **7**, 1233 (1967)